Cold Regions Science and Technology 233 (2025) 104460

Contents lists available at ScienceDirect

Cold Regions Science and Technology

journal homepage: www.elsevier.com/locate/coldregions

Towards accurate ice accretion and galloping risk maps for Quebec: A data-driven approach

Abdeslam Jamali [a], Reda Snaiki [b,*], Ahmed Rahem [a]

[a] Department of Applied Sciences, Université du Québec à Chicoutimi, Chicoutimi, QC, Canada
[b] Department of Construction Engineering, École de Technologie Supérieure, Université du Québec, Montréal, Canada

ARTICLE INFO

Keywords:
Ice accretion
Hazard mapping
Galloping risk
Return periods
Extreme values

ABSTRACT

Ice accretion poses a significant threat to infrastructure and public safety, particularly in regions prone to severe winter weather. Accurate ice accretion hazard mapping is essential for effective risk management and mitigation. While substantial progress has been made in mapping these hazards, most existing ice accretion maps rely on calculated ice accretion values rather than direct measurements, leading to potential inaccuracies. To address these limitations, this study leverages field measurement data from Hydro-Québec's glacimètre network to develop refined ice accretion maps for Quebec. The maximum annual ice accretion thicknesses are extracted, and a rigorous probability distribution fitting analysis is applied to generate 10-, 30-, and 50-year return period values. These values are interpolated using both inverse-distance weighted interpolation (IDWI) and kriging techniques, allowing for a comparative evaluation of interpolation methods. Additionally, galloping risks are assessed using the Performance-Based Ice Engineering (PBIE) framework, producing galloping risk maps for various return periods. By incorporating real-world data and comparing interpolation approaches, this research enhances the accuracy of ice accretion and galloping risk maps, providing more reliable hazard assessments for Quebec's infrastructure.

1. Introduction

Ice accretion on infrastructure, such as power transmission lines, poses a significant hazard in cold climates. Accumulations of ice during freezing rain, wet snow events, and other atmospheric conditions can lead to severe structural failures, power outages, and risks to public safety. This phenomenon is particularly concerning in regions like Quebec, where harsh winter conditions often result in extensive ice buildup. One of the most notable examples is the North American Ice Storm of January 1998, which impacted Canada and the United States. The storm's destructive force led to an estimated $4 billion USD in damages, with over 4 million residents losing power (Mittermeier et al., 2022). Therefore, understanding and predicting ice accretion effects are critical for mitigating risks and ensuring the reliability of essential infrastructure.

Due to the challenges of direct measurement, ice accretion is often estimated using various modelling techniques. Obtaining accurate, widespread data on ice accretion is difficult, as measurement stations are sparse, and ice accretion events are highly localized and dependent on microclimatic conditions. Various models have been proposed to estimate ice accretion, ranging from physics-based to data-driven approaches (Snaiki et al., 2024). Traditional physics-based models of ice accretion rely on simplified mathematical formulations and fundamental physical laws (Goodwin et al., 1983; Makkonen, 1998; Zhang et al., 2012). While these models provide a valuable theoretical framework, they may fall short in capturing the complexities of ice accretion in real-world conditions (He et al., 2021). Data-driven models, on the other hand, leverage diverse data sources, such as the output of numerical models, to establish relationships between input variables (e.g., meteorological conditions, conductor geometry) and ice accretion. These models can be constructed using various machine learning techniques, ranging from simple statistical methods (Chaîné and Castonguay, 1974; Jones, 1998) to complex deep neural networks (Snaiki et al., 2024). While simplified autoregressive formulas offer computational efficiency and ease of implementation, their reliance on predefined basis functions and autoregressive structures may limit their ability to accurately model complex dynamic systems like ice accretion (Jeong et al., 2019; Sheng et al., 2023). Machine learning approaches, such as deep neural networks, provide a promising alternative for rapidly predicting ice accretion. These models can effectively capture

* Corresponding author.
E-mail address: reda.snaiki@etsmtl.ca (R. Snaiki).

https://doi.org/10.1016/j.coldregions.2025.104460
Received 5 November 2024; Received in revised form 3 February 2025; Accepted 16 February 2025
Available online 17 February 2025

nonlinear dynamics without relying on simplified assumptions or linearization, making them well suited for the complex nature of ice accretion (Niu et al., 2017; Ma et al., 2016; Sun and Wang, 2019). While machine learning approaches offer several advantages, they also have certain limitations (Snaiki and Wu, 2022; Wu and Snaiki, 2022). One significant drawback is the reliance on large amounts of high-quality data (Snaiki and Wu, 2019). Insufficient or biased data can lead to inaccurate predictions and limit the generalizability of the models. Additionally, machine learning models can be computationally expensive to train and deploy, especially for complex models with many parameters. Furthermore, deciphering the internal operations of machine learning models can be challenging, making it difficult to understand the underlying physical processes driving ice accretion. This challenge can hinder the development of physically interpretable models that offer insights into these mechanisms.

Ice accretion hazard maps for Canada have been developed to assess the severity and spatial distribution of ice loads due to freezing rain events. Typically based on probabilistic modelling techniques, such as the Gumbel distribution, they estimate extreme ice accretion events over various return periods and have played a crucial role in establishing design standards for Canadian infrastructure. For instance, Yip (1995) generated 30-year return period ice accretion values for a 25 mm diameter rod at various locations across Canada, using the Chaîné and Castonguay (1974) model. Jarrett et al. (2019) also generated 50-year return period ice accretion hazard maps using a 25 mm diameter rod, employing the Gumbel distribution to fit maximum annual ice accretion thickness. Recent advancements in ice accretion hazard mapping have involved the use of multiple ice accretion models and statistical techniques. Sheng et al. (2023) refined and expanded existing hazard maps by applying different models and distributions to various Canadian regions. The Gumbel distribution was found to be suitable for regions prone to ice accretion, while the lognormal distribution was more appropriate for areas with moderate or negligible ice accretion. While significant progress has been made in ice accretion hazard mapping, it's important to note that most existing maps rely on calculated ice accretion values rather than direct measurements. This is due to the inherent challenges of accurately measuring ice accumulation on structural surfaces. The choice of ice accretion model can significantly influence the resulting hazard maps (Sheng et al., 2023), making it difficult to determine the optimal model for all regions.

To overcome the limitations of existing ice accretion models in generating accurate hazard maps, this study leverages field measurement data from Hydro-Québec's extensive glacimètre network to develop refined ice accretion maps for the province of Quebec. By incorporating these field measurements, this research aims to improve the predictive capabilities of current models and provide more reliable assessments of ice storm risks. Maximum annual ice accretion thicknesses were extracted from the glacimètre data for each station and subjected to a comprehensive probability distribution fitting analysis. The resulting 10-, 30-, and 50-year return period values were then interpolated onto a high-resolution map using both inverse-distance weighted interpolation (IDWI) and ordinary kriging techniques. This comparative analysis evaluates the impact of interpolation methods on the accuracy and reliability of the generated ice accretion hazard maps. To further assess the potential risks associated with ice accretion, this study extends the analysis to include galloping risk assessment. The Performance-Based Ice Engineering (PBIE) framework is employed to generate galloping risk maps corresponding to various return periods. The galloping risk is assessed numerically using the double galloping amplitude. The influence of interpolation techniques on the accuracy of these galloping risk maps is also examined.

2. Meteorological data and statistics of ice accretion

2.1. Historical data

This study leverages a comprehensive dataset of ice accretion and wind speed data collected from Hydro-Québec's extensive glacimètre network, established in 1974 (Laflamme, 2004). Strategically located across Quebec, with a particular emphasis on the St. Lawrence Valley, these stations provide detailed measurements of ice accretion on cylindrical surfaces oriented towards each cardinal direction. The glacimètre design allows for precise characterization of icing events, including type, orientation-specific accumulation, thickness, and duration. This rich dataset has served as a cornerstone for developing robust design criteria for overhead transmission line systems in the region, solidifying Hydro-Québec's network as a leading resource for ice accretion research in North America. The present analysis focuses on the period between 1975 and 2020, examining equivalent ice accretion data from 55 stations distributed across Quebec as depicted by Fig. 1. For each station, maximum annual ice accretion thicknesses were extracted and subjected to a rigorous probability distribution fitting analysis. It is important to note that the glacimètre measures the equivalent radial thickness of ice on a 30 mm conductor, assuming a flat terrain (Périard, 2018).

2.2. Probabilistic analysis of ice accretion thickness

To model the extreme ice accretion events, three common probability distributions were considered as proposed by Sheng et al. (2023): the Gumbel, Generalized Extreme Value (GEV), and lognormal distributions. Given the sensitivity of the Generalized Pareto Distribution (GDP) to threshold selection, the peak-over-threshold approach was not employed in this study (Sheng et al., 2023). Fig. 2 illustrates the goodness of fit for these distributions at six representative stations: Iberville, Montréal-A, Québec-A, Saint-Hubert-A, Honfleur and Montmagny. The probability distributions were fitted to the processed ice accretion data using the maximum likelihood estimation method, employing the gumbel_r.fit(), lognorm.fit(), and genextreme.fit() functions from the scipy.stats library in Python. To facilitate visual assessment of the Gumbel distribution, the y-axis was transformed using the function -ln(−ln(CDF)), where CDF denotes the cumulative probabilities of the observed data points. This transformation linearizes the Gumbel distribution when plotted against the transformed y-axis, allowing for a more straightforward visual comparison of the Gumbel, GEV, and lognormal distribution fits.

The results demonstrate significant regional variability in ice accretion, with stations like Honfleur experiencing substantially more severe events compared to those at Montmagny. While both the Gumbel and GEV distributions provided reasonable fits for most stations, the lognormal distribution proved less suitable, particularly for sites like Iberville, Québec-A, and Montmagny. As illustrated in Fig. 2, the choice of the most appropriate distribution is site-specific. While the Gumbel

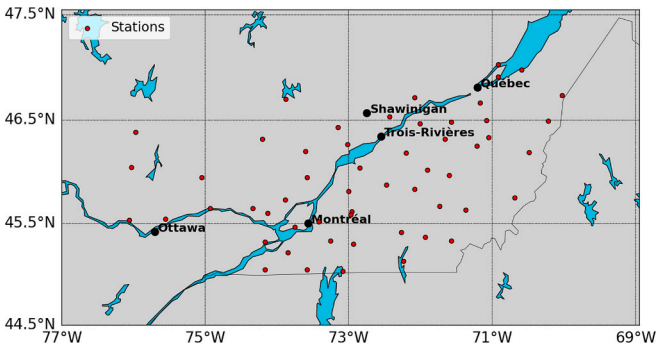

Fig. 1. Glacimètre station network in Quebec

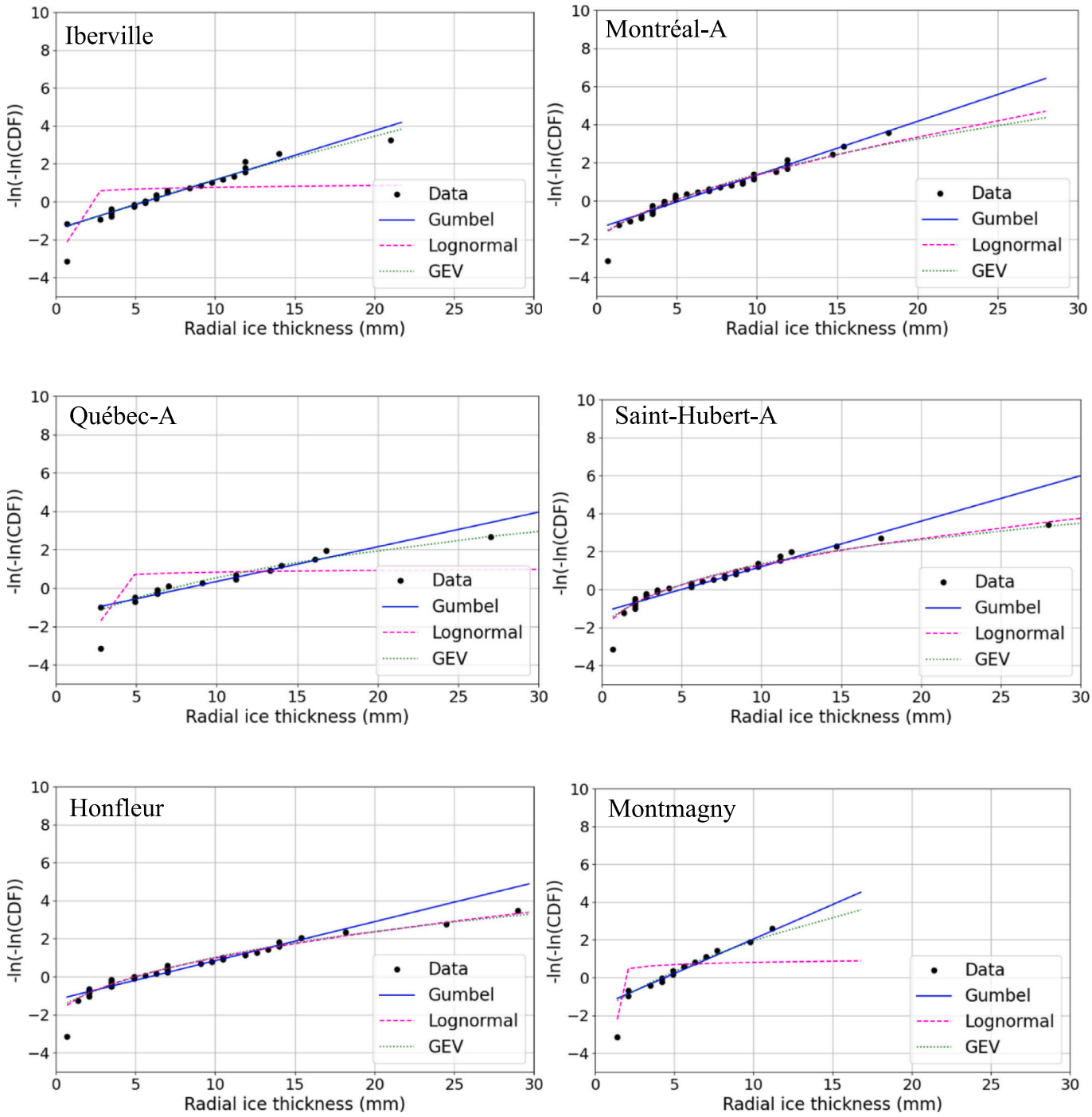

Fig. 2. Probability distribution fitting for a maximum annual ice accretion thickness.

distribution offered a reasonable fit at several locations (e.g., Iberville, Montréal-A and Montmagny), the GEV distribution offered superior performance, particularly at the Québec-A, Saint-Hubert-A, and Honfleur stations. Furthermore, as discussed by Lu and Chakrabarti (2016, 2023), alternative distributions, such as the modified Gumbel distribution, may provide a better characterization of extreme value behavior, particularly with longer records. An extended dataset would enable a more rigorous assessment of tail behavior and facilitate the precise selection of the optimal distribution. In this study, the Gumbel distribution was selected as a suitable representation of the available data. However, it is recognized that this selection may not be optimal for all stations, and further analysis with more extensive datasets could lead to more refined choice of distribution.

3. Ice accretion hazard maps

To determine the T-year return period value of the annual maximum ice accretion thickness (I_T), the following equation was employed (Sheng et al., 2023):

$$1-\frac{1}{T}=p_0+(1-p_0)F_I(I_T) \tag{1}$$

where p_0 represents the probability of zero ice accretion, and $F_I(I_T)$ denotes the fitted distribution. The calculated T-year return period values were then interpolated onto a high-resolution map using both inverse-distance weighted interpolation (IDWI) and ordinary kriging

techniques.

The IDWI and kriging are two commonly used spatial interpolation methods for estimating values at unmeasured locations based on known data points. The IDWI is a deterministic spatial interpolation technique that estimates values at unobserved locations by calculating a weighted average of observed values at neighboring points (Shepard, 1968; Apaydin et al., 2004; Davalos et al., 2023). The weights assigned to each observed value are inversely proportional to the distance separating the known and unknown locations, effectively giving greater influence to closer observations. The general formulation of IDWI is expressed as:

$$Z(x) = \frac{\sum_{i=1}^{N} \omega_i Z_i}{\sum_{i=1}^{N} \omega_i} \tag{2}$$

where $Z(x)$ is the estimated value, Z_i are the observed values, ω_i are the weights (typically $\omega_i = 1/d_i^p$, where d_i is the distance to the known point and p is a power parameter), and N is the number of neighboring points considered. IDWI is computationally efficient but does not account for spatial correlation between points.

Kriging is a geostatistical interpolation technique that accounts for both the distance and the spatial correlation between data points to estimate values at unobserved locations (Cressie, 1990; Nygaard et al., 2014). It is based on the assumption that spatial variation can be represented by a stochastic process with a defined spatial structure. A key component of Kriging is the semivariogram, which quantifies this spatial correlation. This information is then used to derive optimal weights for neighboring observations, minimizing the estimation variance. The general form of the Kriging estimator is given by:

$$Z(x) = \sum_{i=1}^{N} \lambda_i Z_i \tag{3}$$

where λ_i are weights determined by solving a system of equations based on the semivariogram model. Kriging generally provides smoother and more statistically robust estimates compared to IDWI but requires more computational effort and a well-defined spatial correlation structure.

Both methods are applied to generate ice accretion hazard maps in this study, allowing for a comparative evaluation of their effectiveness. Specifically, the maximum annual ice accretion thicknesses for 10, 30, and 50-year return periods were estimated and visualized using these interpolation methods in Figs. 3, 4 and 5, respectively.

The generated ice accretion hazard maps clearly depict significant spatial variability across the region. A pronounced trend of increased ice thickness near the St. Lawrence River is evident, suggesting that these areas are more susceptible to severe icing events compared to other regions. This observation underscores the influence of geographical and climatic factors, such as proximity to water bodies, prevailing winds, and terrain elevation, on ice accretion patterns. As expected, the ice thickness increases with increasing return periods, maintaining a generally consistent spatial pattern but with varying magnitudes. For example, the 50-year return period map (Fig. 5) exhibits a maximum ice accretion of 22 mm, while the 10-year return period map (Fig. 3) shows a maximum of 10 mm using the kriging approach. Interestingly, the kriging technique produces smoother maps compared to the IDWI technique. However, IDWI tends to yield slightly higher ice accretion values. For instance, at the 50-year return period (Fig. 5), IDWI estimates a maximum of 25 mm compared to 22 mm from kriging. Similar differences are observed for the 30- and 10-year return periods. Despite these minor discrepancies, the overall spatial distribution of ice accretion remains consistent across all three return periods, reflecting the underlying geographical and climatic influences. The choice of interpolation technique may introduce some variability in the specific values, but the general patterns and trends remain reliable for assessing ice accretion risk in the region.

4. Galloping risk maps for Quebec

This section assesses the risk of galloping-induced vibrations on iced conductors, leveraging the ice accretion hazard maps developed in Sect. 3 and wind maps, as illustrated in Fig. 6. The assessment follows a two-stage process: (1) an evaluation of conditions necessary to galloping, and (2) the application of a galloping model to estimate risk where these conditions are met. This approach directly links the ice accretion hazard maps to the estimation of galloping risk, addressing a critical aspect of power line vulnerability to extreme weather events. To assess the risk of galloping-induced vibrations on iced conductors, this section leverages the ice accretion hazard maps developed in Sect. 3. The Performance-Based Ice Engineering (PBIE) framework, a recently developed

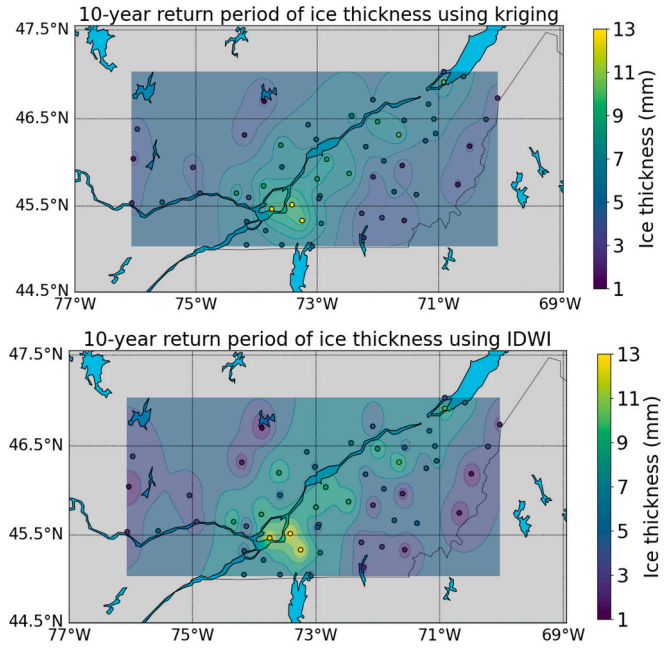

Fig. 3. Comparison of kriging and IDWI for estimating ice accretion hazard in Quebec (10-year return period).

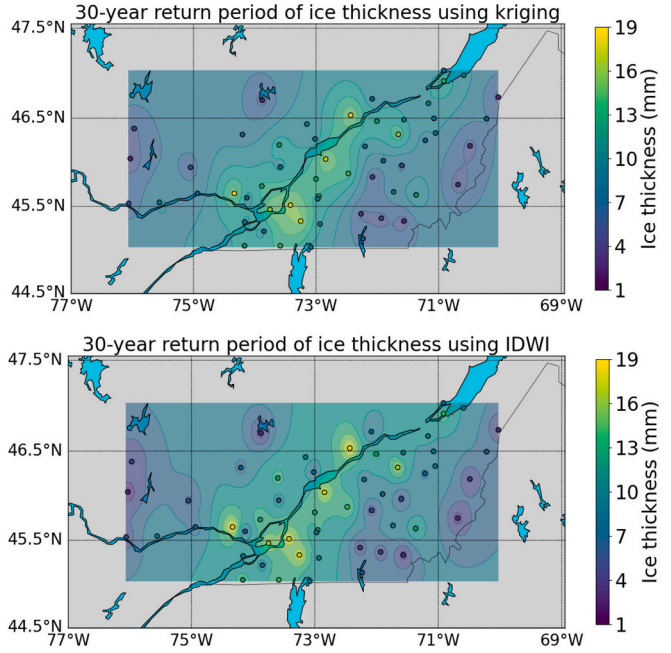

Fig. 4. Comparison of kriging and IDWI for estimating ice accretion hazard in Quebec (30-year return period).

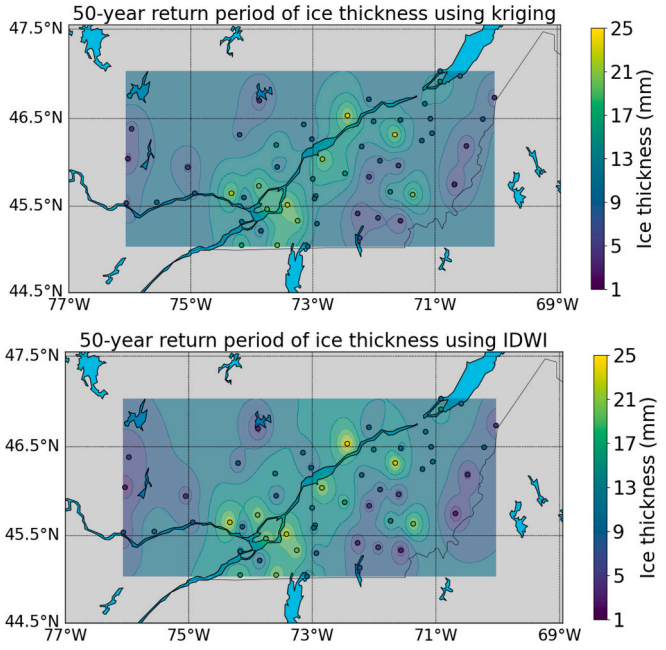

Fig. 5. Comparison of kriging and IDWI for estimating ice accretion hazard in Quebec (50-year return period).

approach for evaluating ice storm risks, is employed to generate galloping risk maps corresponding to various return periods (Snaiki, 2024). The PBIE framework, designed for both local and regional applications, utilizes advanced data-driven techniques, such as machine learning, to efficiently predict risks like galloping. By sequentially assessing hazards, structural interactions, and potential damage, the PBIE enables real-time risk estimation across extensive areas. Its versatility extends to various structures, from transmission lines to wind turbines, supporting both emergency response and long-term planning in the face of climate change. The galloping amplitude of transmission lines subjected to wind and ice is estimated using a simplified semi-empirical approach (Lu and Chan, 2009; Lu and Chakrabarti, 2023). While more sophisticated theories can be integrated into the PBIE framework, this simplified model provides a practical means of assessing galloping-induced risk. The galloping risk will be quantified in terms of the double galloping amplitude. A concise overview of galloping instability, conditions, and the employed dynamic model will be presented in the subsequent sections.

4.1. Galloping instability and conditions

Galloping is a type of wind-induced instability that can result in significant, low-frequency oscillations in transmission lines, particularly when ice accretion is present. To predict the onset of galloping, two primary criteria must be satisfied (den Hartog, 1932). The first criterion involves the Den Hartog coefficient, a_g, which must be negative:

$$a_g = C_d + \frac{dC_l}{d\alpha} < 0 \tag{4}$$

where C_d represents the drag coefficient, C_l denotes the lift coefficient, and α is the angle of attack. The second criterion for galloping instability pertains to the total system damping, ζ, which must satisfy the following inequality:

$$\xi = \xi_s + \xi_a < 0 \tag{5}$$

where ξ_s represents structural damping and ξ_a denotes aerodynamic damping. To fulfill the second criterion for galloping instability, the wind speed must exceed a critical wind speed value, denoted as V_c, which can be calculated using the following expression:

$$V_c = -\frac{4.\omega_n.\xi_s.m_s}{\rho_0.d_c.a_g} \tag{6}$$

where ω_n represents the natural angular frequency, m_s is the mass of the conductor, ρ_0 denotes the density of ice and d_c is the conductor's diameter.

4.2. Dynamic model of the transmission line system

A semi-empirical modelling approach is used in this study to simulate the galloping amplitude of transmission lines under various wind and ice loading conditions (Lu and Chan, 2009; Lu and Chakrabarti, 2023). This methodology, which integrates finite element analysis and a 3-degree-of-freedom system, provides a computationally efficient and accurate means of assessing galloping behavior. The model has been rigorously validated against comprehensive parametric studies and field measurements from North American transmission systems. The resulting

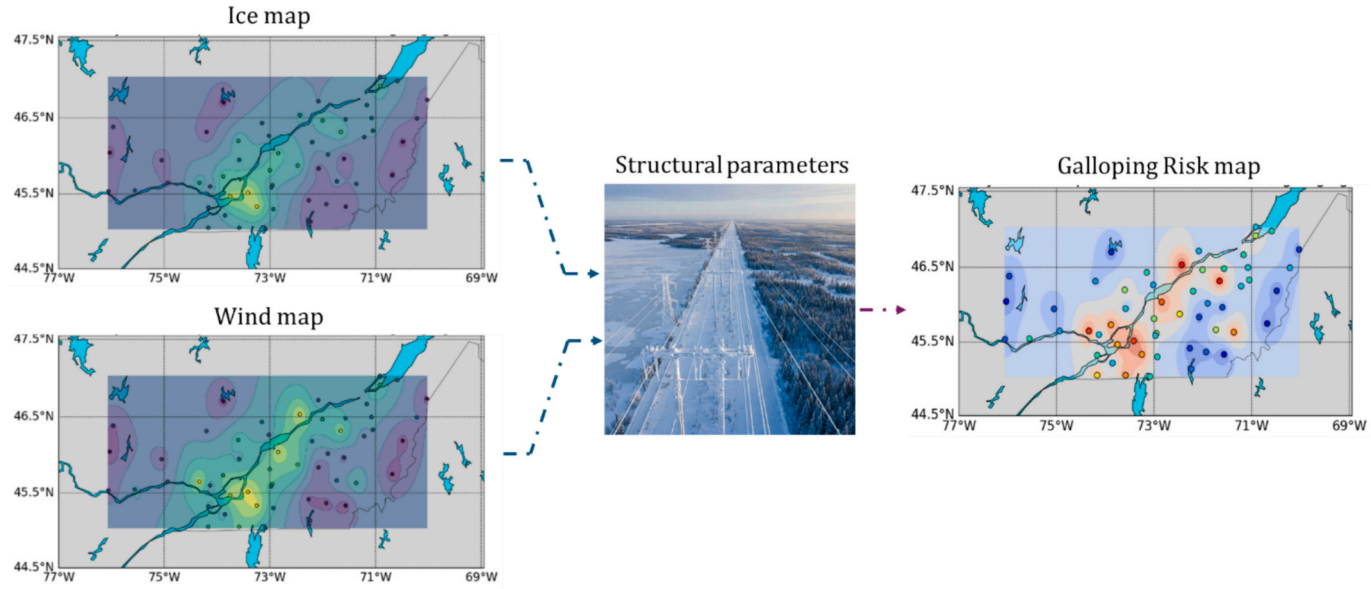

Fig. 6. Conceptual schematic for galloping risk assessment

semi-empirical equation, presented below, enables the estimation of galloping amplitudes for both single and bundled conductors, regardless of support type (suspension or dead-end). The vertical galloping amplitude, denoted as A_G, is calculated as follows (Lu and Chan, 2009):

$$A_G = G/f \tag{7}$$

The galloping factor, G, characterizing the severity of galloping, is typically assigned a value of 0.75 m/s for North American transmission lines based on extensive field observations. The natural frequency of the conductor in the vertical direction, denoted as f, is a critical factor in determining galloping susceptibility. For sagged conductor spans with fixed-end conditions, f can be calculated using the following equation (Lu and Chan, 2009):

$$f = \frac{k}{L}\sqrt{\frac{H}{m}} \tag{8}$$

The natural frequency f is influenced by several factors, including the conductor span length L, static tension H, mass per unit length m, and a parameter k related to the number of galloping loops. For a one-loop galloping mode, k can be determined as a function of the conductor tension (T) by the following equation (Lu and Chan, 2009):

$$tan(k\pi) = k\pi - \frac{4(k\pi)^3}{K_c\frac{L^3}{T^3}m^2g^2} \tag{9}$$

The conductor stiffness, K_c, is calculated as the product of the equivalent elastic modulus E and the cross-sectional area A, divided by the span length L. The single galloping amplitude serves as a basis for determining the double galloping amplitude Y, which can be expressed as $Y = 2A_G$.

4.3. Galloping risk maps

The PBIE framework was utilized to evaluate the risk of vertical galloping on iced conductors, considering ice accretion scenarios corresponding to return periods of 10 and 30 years, as delineated in Sect. 3. To assess the influence of interpolation technique, design maps were generated using both ordinary kriging and inverse-distance weighted interpolation (IDWI). Limit states (LS) were established based on the double galloping amplitude, Y, and defined as the difference between engineering demand and structural capacity for each damage state. A limit state of $LS \geq 0$ indicates failure. Three risk categories were defined according to the magnitude of Y: low-risk ($Y \leq 2\,m$), moderate-risk ($2 < Y \leq 3\,m$), and high-risk ($Y > 3\,m$).

It is well documented that ice accretion on fixed conductors often exhibits a crescent-shaped profile. Consequently, accurate modelling of this profile is crucial for realistic representation of wind-induced aerodynamic loads. Consistent with previous research (Rossi et al., 2020; Davalos et al., 2023; Snaiki, 2024), a semi-elliptical shape was adopted to model the ice accretion. The drag coefficient was determined based on experimental wind tunnel data from Rossi et al. (2020). Other relevant structural parameters included: $L = 172.4m$, $E = 70GPa$, $sag = 3.39m$, $m = 1.3kg/m$, and $A = 4.35{*}10^{-4}m^2$. To incorporate uncertainties in the structural parameters within the PBIE framework, a limited number of parameters were treated as random variables. Specifically, the conductor diameter was assumed to follow a normal distribution with a mean of 23.55 mm and a coefficient of variation of 0.05. The modulus of elasticity was modeled as a log-normal distribution with a mean of 70 GPa and a coefficient of variation of 0.03. Wind hazard maps, corresponding to the same return periods as the ice accretion maps, were developed using a comparable methodology to assess the potential for galloping. Fig. 7 illustrates the galloping risk maps for return periods of 10 and 30 years, generated using ordinary kriging interpolation.

The galloping risk maps, corresponding to return periods of 10 and 30 years, provide valuable insights into the spatial distribution and severity of galloping risk within the region. Analysis of these maps enables the identification of critical areas, facilitating the assessment of potential infrastructure impacts and informed decision-making for risk mitigation. While the overall spatial distribution of risk remains relatively consistent across all return periods, specific regions, such as the St. Lawrence Valley, particularly in the southern portion, consistently exhibit higher risk levels for all three risk categories. This is attributable to the same underlying factors influencing galloping susceptibility, including topography and meteorological conditions. Although the

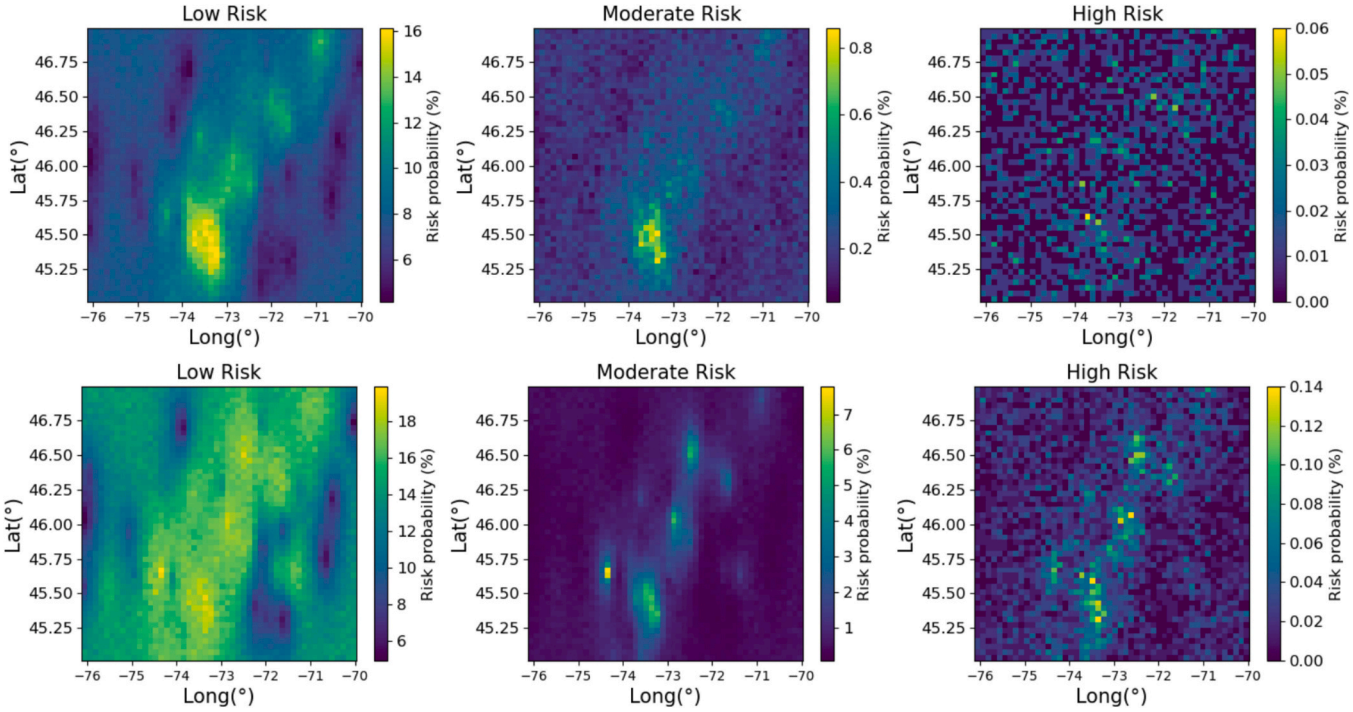

Fig. 7. Galloping-induced risk maps estimated for 10 years (top) and 30 years (bottom) return periods using kriging interpolation.

general risk pattern persists, notable variations in risk level intensity are evident. For example, in the southern part of the St. Lawrence Valley (near the island of Montreal), the risk probability for the low-risk category increases from approximately 16 % for a 10-year return period to nearly 20 % for a 30-year return period. Similarly, the risk probability in the same region for the high-risk category increases from approximately 0.06 % to 0.14 % over the same return period. Similar maps were also generated using the IDWI technique, as depicted in Fig. 8.

The overall spatial distribution of risk remains consistent between the IDWI and ordinary kriging maps. Despite overall similarities in the risk maps generated using different interpolation techniques, notable variations in risk intensity were observed. IDWI maps generally produced higher risk values compared to ordinary kriging. For a 10-year return period, the risk probability for the low-risk category was approximately 16 % when using kriging, but increased to 17 % when using IDWI. Similarly, for the high-risk category and a 10-year return period, the risk probability increased from 0.06 % for kriging to 0.085 % for IDWI. The choice of interpolation technique can influence the smoothness and detail of the generated maps. IDWI, being a distance-based method, may introduce more localized variations in risk, especially in areas with sparse data. Ordinary kriging, on the other hand, tends to produce smoother maps by considering the spatial correlation between data points.

5. Discussion

This study developed ice accretion and galloping risk maps for Quebec, providing valuable insights into regional hazards and informing infrastructure resilience planning. Historical ice accretion data from Hydro-Québec's glacimètre network were analyzed, and ice accretion events were modeled using various probability distributions, including Gumbel, Generalized Extreme Value (GEV), and lognormal distributions. Ice accretion hazard maps were then generated for 10, 30, and 50-year return periods using inverse distance weighted interpolation (IDWI) and kriging. Subsequently, galloping risk was assessed using the Performance-Based Ice Engineering (PBIE) framework. Due to the limited availability of detailed grid topology and structural parameters, a simplified structural model for conductors was employed. Galloping risk maps were produced for the 10 and 30-year return periods, highlighting areas of elevated risk. The results clearly demonstrate the significant spatial variability in both ice accretion and galloping risk across Quebec, underscoring the importance of accurate hazard assessment for infrastructure resilience.

Despite the advancements presented in this study, certain limitations must be considered. The choice of probability distribution for modelling extreme ice accretion is inherently location-dependent. Although the Gumbel distribution was selected for its general applicability, alternative distributions, such as the GEV or modified Gumbel distributions, may provide a better fit for specific locations, particularly in capturing the tail behavior of extreme events. Longer data records are needed to refine this selection and reduce uncertainty in extreme value estimation. Furthermore, while the galloping risk analysis generally suggests increasing risk with longer return periods, this relationship is not always straightforward. The aerodynamic instability that leads to galloping is strongly influenced by the shape of the ice accretion on the conductor. This study assumed a worst-case scenario, where ice accretion predominantly forms a crescent shape, known to exacerbate galloping. However, more severe ice accretion events, such as those associated with a 50-year return period, may result in more circular ice cross-sections, potentially reducing the aerodynamic forces driving galloping. Predicting the precise ice shape for a given return period is a complex challenge, dependent on a multitude of meteorological and physical factors. Consequently, this study focused on the 10 and 30-year return periods, excluding the 50-year return period from the galloping risk analysis. Future research should prioritize incorporating ice shape variability into galloping risk assessments to provide a more comprehensive evaluation of transmission line stability under extreme ice loading conditions.

In addition, overlaying geographic features, such as topography, vegetation, and land use, onto the risk maps would provide valuable context and facilitate a deeper understanding of the factors influencing galloping risk. Identifying correlations between environmental

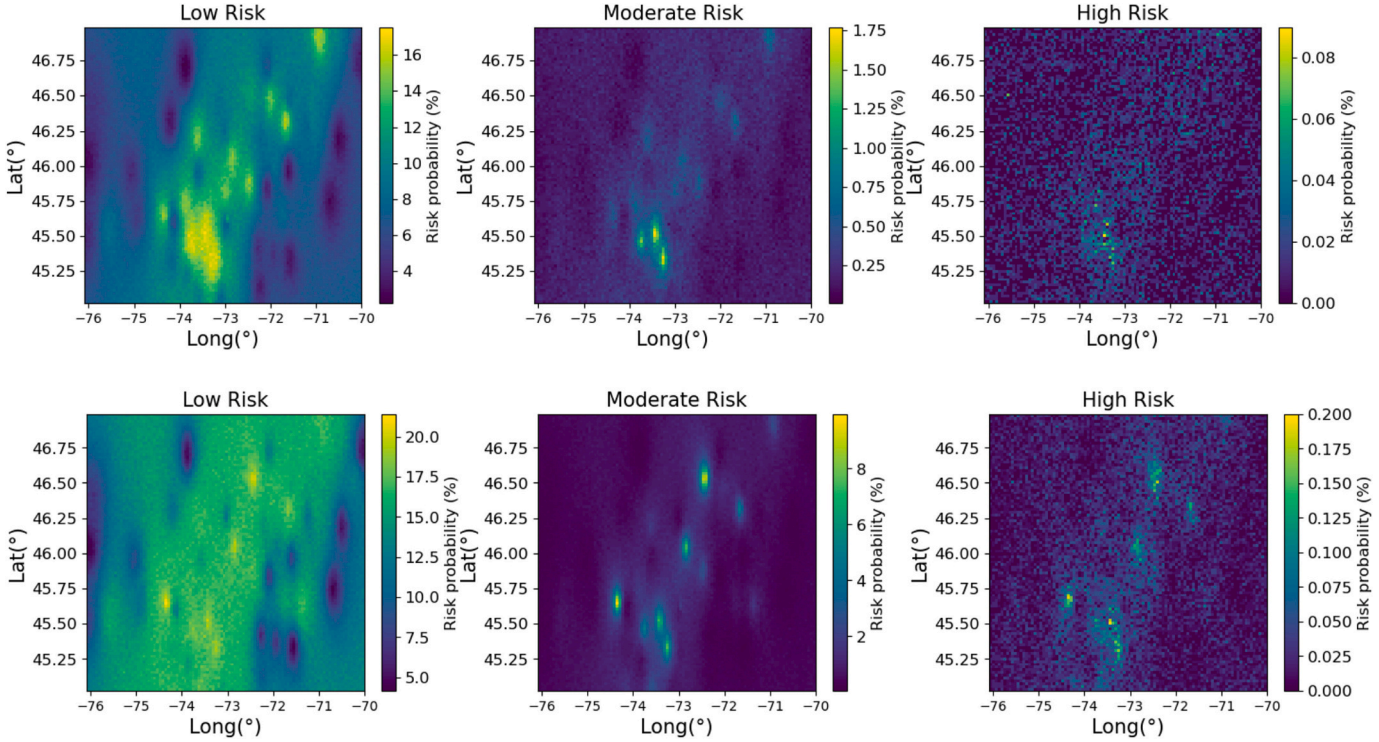

Fig. 8. Galloping-induced risk maps estimated for 10 years (top) and 50 years (bottom) return periods using the IDWI technique.

conditions and risk levels can inform targeted mitigation strategies. The accuracy of the risk assessment is inherently dependent on the quality of the input data, including meteorological data, conductor characteristics, and ice accretion models. The galloping risk assessment model itself may also have limitations in capturing all relevant factors and scenarios. For example, this study employed a simplified semi-empirical modelling approach to simulate galloping amplitudes, and a uniform grid network was assumed due to data limitations. A more rigorous approach would integrate the precise layout of transmission lines within the Performance-Based Ice Engineering (PBIE) framework. Additionally, the potential impacts of climate change on the frequency and severity of galloping events should be considered in future risk assessments. Incorporating climate change projections is crucial for long-term infrastructure planning (Snaiki and Parida, 2023).

Despite these limitations, the generated ice accretion and galloping risk maps provide valuable tools for prioritizing areas for risk assessment, inspection, and maintenance. Regions identified as consistently high-risk should be prioritized for targeted inspections and mitigation measures. These measures could include conductor modifications, improved ice management practices, or the installation of galloping dampers. The maps offer critical information for long-term planning, enabling informed infrastructure upgrades and risk-based decision-making for enhanced grid resilience.

6. Concluding remarks

In this study, an enhanced methodology was proposed for generating ice accretion and galloping risk maps for Quebec by utilizing real-world field measurement data from Hydro-Québec's glacimètre network. By combining maximum annual ice accretion values with interpolation techniques, such as inverse distance weighting and kriging, accurate maps were developed for 10-, 30-, and 50-year return periods. Furthermore, by applying the Performance-Based Ice Engineering (PBIE) framework, the analysis was extended to include galloping risk, a critical factor for transmission line safety under severe icing conditions. The results indicate significant spatial variability in both ice accretion and galloping risk across the province, particularly in the St. Lawrence Valley region. This study highlights the importance of using field measurement data to improve the accuracy and reliability of hazard maps. It also underscores the influence of interpolation methods on risk predictions, emphasizing the need for careful selection of modelling techniques based on regional characteristics. Future work should focus on refining these methods and integrating climate change projections to ensure long-term resilience of critical infrastructure in ice-prone regions.

CRediT authorship contribution statement

Abdeslam Jamali: Writing – review & editing, Writing – original draft, Visualization, Validation, Software, Methodology, Investigation, Formal analysis, Data curation, Conceptualization. **Reda Snaiki:** Writing – review & editing, Writing – original draft, Visualization, Validation, Supervision, Software, Resources, Project administration, Methodology, Investigation, Funding acquisition, Formal analysis, Conceptualization. **Ahmed Rahem:** Writing – review & editing, Validation, Supervision, Methodology, Investigation, Formal analysis, Conceptualization.

Declaration of competing interest

The authors declare that they have no known competing financial interests or personal relationships that could have appeared to influence the work reported in this paper.

Data availability

The authors do not have permission to share data.

Acknowledgements

This work was partly supported by the Natural Sciences and Engineering Research Council of Canada (NSERC) [grant number CRSNG RGPIN 2022-03492].

References

Apaydin, H., Sonmez, F.K., Yildirim, Y.E., 2004. Spatial interpolation techniques for climate data in the GAP region in Turkey. Clim. Res. 28 (1), 31–40.
Chaîné, P.M., Castonguay, G., 1974. New Approach to Radial Ice Thickness Concept Applied to Bundle-like Conductors, vol. 4. Environment Canada, Atmospheric Environment.
Cressie, N., 1990. The origins of kriging. Math. Geol. 22, 239–252.
Davalos, D., Chowdhury, J., Hangan, H., 2023. Joint wind and ice hazard for transmission lines in mountainous terrain. J. Wind Eng. Ind. Aerodyn. 232, 105276.
Den Hartog, J.P., 1932. Transmission line vibration due to sleet. Trans. Am. Inst. Electr. Eng. 51 (4), 1074–1076.
Goodwin, T., Mozer, J.D., DiGioia, A.M., Power, B.A., 1983, June. Predicting ice and snow loads for transmission line design. In: Proc. first Int. Workshop on Atmospheric Icing of Structures (pp. 267-273).
He, L., Luo, J., Zhou, X., 2021, March. A novel deep learning model for transmission line icing thickness prediction. In: In 2021 IEEE 5th Advanced Information Technology, Electronic and Automation Control Conference (IAEAC), vol. 5. IEEE, pp. 733–738.
Jarrett, P., Yau, K.H., Morris, R., 2019, June. Update of the reference ice thickness amounts due to freezing rain for Canadian codes and standards. In: Proceedings of the International Workshop on Atmospheric Icing of Structures (pp. 23-28).
Jeong, D.I., Cannon, A.J., Zhang, X., 2019. Projected changes to extreme freezing precipitation and design ice loads over North America based on a large ensemble of Canadian regional climate model simulations. Nat. Hazards Earth Syst. Sci. 19 (4), 857–872.
Jones, K.F., 1998. A simple model for freezing rain ice loads. Atmos. Res. 46 (1–2), 87–97.
Laflamme, J., 2004. La mesure des dépôts de verglas. Rapport interne (d'Hydro-Québec).
Lu, M.L., Chakrabarti, D., 2016. Estimating Extreme Ice on Power Line by Modified Gumbel distribution. CIGRE Canada Conference, Vancouver, BC, 2016.
Lu, M.L., Chakrabarti, D., 2023. Design ice and wind on overhead transmission lines in British Columbia. Cold Reg. Sci. Technol. 214, 103960.
Lu, M.L., Chan, J.K., 2009. A Rational Design Equation for Galloping Power Lines. In: Int. Conference on Ultra-High Voltage Transmission, Beijing, China.
Ma, T., Niu, D., Fu, M., 2016. Icing forecasting for power transmission lines based on a wavelet support vector machine optimized by a quantum fireworks algorithm. Appl. Sci. 6 (2), 54.
Makkonen, L., 1998. Modeling power line icing in freezing precipitation. Atmos. Res. 46 (1–2), 131–142.
Mittermeier, M., Bresson, E., Paquin, D., Ludwig, R., 2022. A deep learning approach for the identification of long-duration mixed precipitation in Montréal (Canada). Atmosphere-Ocean 60 (5), 554–565.
Niu, D., Wang, H., Chen, H., Liang, Y., 2017. The general regression neural network based on the fruit fly optimization algorithm and the data inconsistency rate for transmission line icing prediction. Energies 10 (12), 2066.
Nygaard, B.E.K., Seierstad, I.A., Veal, A.T., 2014. A new snow and ice load map for mechanical design of power lines in Great Britain. Cold Reg. Sci. Technol. 108, 28–35.
Périard, G., 2018. Rapport glacimétrique saison 2018–2019. Rapport interne (d'Hydro-Québec).
Rossi, A., Jubayer, C., Koss, H., Arriaga, D., Hangan, H., 2020. Combined effects of wind and atmospheric icing on overhead transmission lines. J. Wind Eng. Ind. Aerodyn. 204, 104271.
Sheng, C., Tang, Q., Hong, H.P., 2023. Estimating and mapping extreme ice accretion hazard and load due to freezing rain at Canadian sites. Int. J. Disaster Risk Sci. 14 (1), 127–142.
Shepard, D., 1968. A two-dimensional interpolation function for irregularly-spaced data. In: Proceedings of the 1968 23rd ACM national conference, pp. 517–524.
Snaiki, R., 2024. Performance-based ice engineering framework: a data-driven multi-scale approach. Cold Reg. Sci. Technol. 224, 104247.
Snaiki, R., Parida, S.S., 2023. A data-driven physics-informed stochastic framework for hurricane-induced risk estimation of transmission tower-line systems under a changing climate. Eng. Struct. 280, 115673.
Snaiki, R., Wu, T., 2019. Knowledge-enhanced deep learning for simulation of tropical cyclone boundary-layer winds. J. Wind Eng. Ind. Aerodyn. 194, 103983.
Snaiki, R., Wu, T., 2022. Knowledge-enhanced deep learning for simulation of extratropical cyclone wind risk. Atmosphere 13 (5), 757.
Snaiki, R., Jamali, A., Rahem, A., Shabani, M., Barjenbruch, B.L., 2024. A metaheuristic-optimization-based neural network for icing prediction on transmission lines. Cold Reg. Sci. Technol. 224, 104249.

Sun, W., Wang, C., 2019. Staged icing forecasting of power transmission lines based on icing cycle and improved extreme learning machine. J. Clean. Prod. 208, 1384–1392.
Wu, T., Snaiki, R., 2022. Applications of machine learning to wind engineering. Front. Built Environ. 8, 811460.
Yip, T.C., 1995. Estimating icing amounts caused by freezing precipitation in Canada. Atmos. Res. 36 (3–4), 221–232.
Zhang, Z., Huang, H., Jiang, X., Hu, J., Sun, C., 2012. Analysis of ice growth on different type insulators based on fluid dynamics. Diangong Jishu Xuebao(Transactions of China Electrotechnical Society) 27 (10), 35–43.